GPR and LiDAR Synergy: Honeycomb detection in Concrete Structures

R.Subakaran
Department of Civil Engineering
University of Moratuwa
Moratuwa, Sri Lanka
haranniro@gmail.com

Sumudu Herath
Department of Civil Engineering
University of Moratuwa
Moratuwa, Sri Lanka
sumuduh@uom.lk

***Abstract*— Honeycombs are formed due to trapped air voids around the coarse aggregates during concreting. These can form inside the concrete structures and on the surface as well. Detecting honeycomb concrete structures is essential to ensure the structural integrity and durability of the structure. However, detecting internal honeycombs are much cumbersome as it is not visible to naked eyes. Ground Penetrating Radar (GPR) is a system that emits and receives Electromagnetic waves which can penetrate through different materials and could detect any disturbances on its travel path. Using the GPR output data, we can identify the defects, honeycombs. Further, Laser imaging Detection and Ranging (LiDAR) emits and receives Laser waves to acquire surface details and reconstruct 2.5D models as Point Clouds. Each of these systems has individual drawbacks. By combining both the systems we can produce data sets that can be used to reconstruct a full 3D understanding of the structure and to conduct further analysis. This paper reviews the pros and cons of GPR and LiDAR and proposes a method on how a full 3D understanding can be obtained using both of these systems and the limitations in the real-world applications of this synergy.**

Keywords— Honeycombs in Concrete, GPR, LiDAR, Point Clouds, NDT, Concrete Defects, Photogrammetry

I. INTRODUCTION

Honeycombs are air voids that are trapped inside the concrete due to the effect of segregation [1]. These can be formed on the concrete surface as well and they become visible to naked eyes as the formworks are removed. Improper vibration, presence of larger size aggregates and using stiff concrete can cause Honeycombing in concrete [3]

Surface honeycombs affect the aesthetics and can be easily recovered but internal honeycombs can lead to the reduction of load-carrying capacity and affect the permeability of the elements. Detecting the honeycombs are still challenging since they form in various sizes, shapes and positions. Honeycombs can be formed as a continuous channel causing severe water penetration and they are critical in Water Retaining Structures and Tunnels [1]. Laser imaging Detection and Ranging (LiDAR) and Ground Penetrating Radar (GPR) are two technologies or rather tools that are used independently and abundantly in many Civil Engineering related principles for two distinctly different purposes. Though both of those technologies have added significant benefits to the industry, they have their own drawbacks as well, but the drawbacks of those individual technologies can be eliminated by using both in combination during projects.

GPR works on the basic principle of reflection of Electromagnetic Waves [4]. One of many uses of GPR is performing various Non-destructive Tests in various materials. Even though GPR has tremendous advantages such as quick data acquisition and detects various elements underneath it, the main drawback is the complexity of the output [5]. The rebars which generally lies near the surface of the majority of the concrete structures, produce stronger reflections, which interrupts weaker reflections from underneath flaws [2]. In the absence of rebars, in structures made up of masonry or mass concrete, they work fine and are able to detect air voids. In Fig. 1, a GPR output obtained during a masonry unit survey is shown and the reflections from a void inside the masonry panel are noticeable at a depth of 20cm and 43cm. Two reflections represent the starting boundary of the void and the finishing boundary of the void respectively.

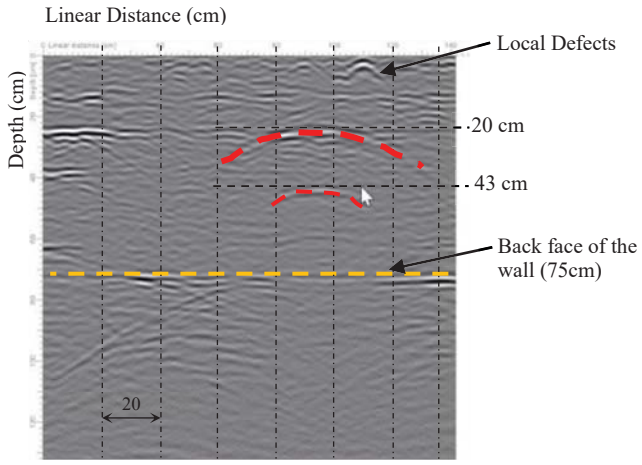

Fig. 1. The result obtained from a GPR survey done on a masonry unit.

Meanwhile, according to [2], using the GPR in transmission mode than reflection mode reduced the attenuation caused by the rebars and have provided promising results to detect voids in structures which has access from opposite sides. Fig. 2 (a) shows the test specimen used by [2] and Fig. 2 (b) represents the output GPR data when it is used in the transmission mode configuration than in the reflection mode configuration and it can be clearly seen that the disturbances caused by the rebars are eliminated to a greater extent and it has shown the size effect of the voids in the output.

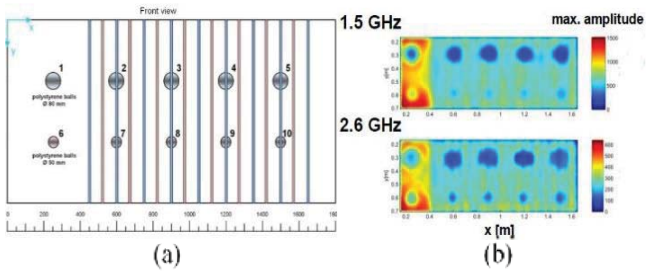

Fig. 2. (a) Test specimen (b) GPR output.

Meanwhile, on the other hand, LiDAR emits and receives laser pulses to reconstruct the surface model. This is widely used in the Civil Engineering industry to produce Digital Twin of structures [6]. The faster scanning time, precision and accuracy of the laser scanning systems are some notable advantages [8, 7], but it cannot penetrate through surfaces and extract features underneath the surface. Therefore, the subsurface conditions would not be detected in LiDAR scan outputs but only in the surface conditions.

Output from LiDAR can be obtained in the form of Point Clouds. A Point Cloud is a set of points in the 3-dimensional space with semantic information embedded in each point in the data set [7, 21]. Photogrammetry is an easy and inexpensive technique from which the point cloud data can be obtained by combining several photos and videos of structures using commercially available software. The reconstructed models using Photogrammetry or LiDAR is called a 2.5D representation [9]. In Fig. 3 the point cloud representation of a retaining wall structure is shown. This is created using 36 images using Agisoft Metashape software.

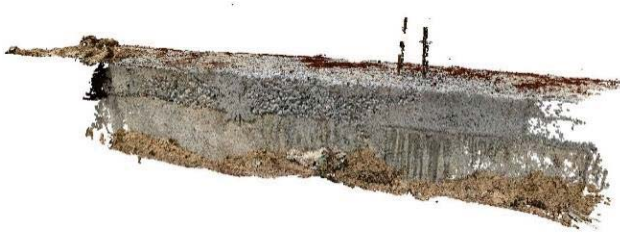

Fig. 3. Point Cloud representation of a retaining wall, reconstructed using Agisoft Metashape.

The drawback of LiDAR technology is the inefficiency to reconstruct features underneath the surface but it is well known to reconstruct surface features and produce point cloud data [21]. This paper is concentrated on how to improve the LiDAR point cloud data to reconstruct a complete 3D point cloud understanding of a structure when combined with GPR data and to detect and identify honeycombs in concrete.

II. Review of Existing Technique

A. Data Collection Techniques

GPR data collections are done both manually and automatically. For any scanning, firsts the scan location is analysed and a grid of particular spacing is chosen, such that the GPR scanner is passed over individual grid lines. The selection of grid density depends on the accuracy and density of the data required. Usually, the GPR scanners are scanned in two perpendicular directions, because the scanners that are commonly available in the market can acquire data along a single direction, whereas there are advanced scanners that do not require scanning in two different directions at one pass as well. There is a variety of equipment available in the industry for various purposes, for scanning Highway Road pavements, an automobile mounted with a GPR system [12], as shown in Fig. 4. Meanwhile, there are handheld and compact scanners as well for small-scale tasks or applications.

Fig. 5. A standard vehicle used for mobile surveys, image source [12]

B. Data Processing and Interpretation

After the scanning process has finished, the data require postprocessing, where the data is converted to a more usable and understandable format, often they are converted as the amplitude representation of the reflected waves plotted against distance along with the wave propagation. Fig. 5 shows raw data and the post-processed data of a scanning project.

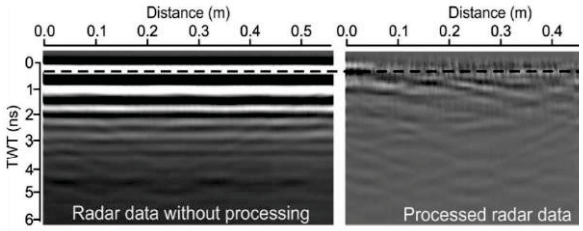

Fig. 6. Raw data (left) and the processed data (right) of a scan done on a test slab, image source [13]

But the post-processed data too require substantial prior knowledge about the data interpretation. While scanning a hypothetical slab element, where there is no other disturbance causing elements in the subsurface region other than the reinforcements, the data interpretation would be straightforward, because the reflections are only due to the presence of reinforcements. Fig. 6 which is obtained as a result of a scan done on a concrete bridge deck indicates the series of reinforcements underneath the top surface [10].

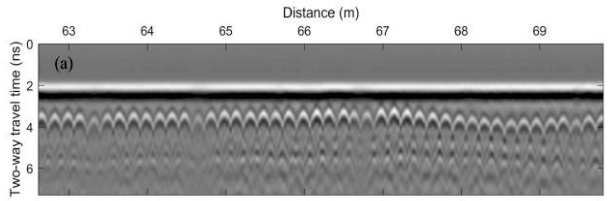

Fig. 4. Processed data showing a series of reinforcements in the subsurface. image source [10]

Usually, this may not be the actual case, there could be many unknown subsurface disturbances in a single element, such as voids, separations, cracks, reinforcements, variation in materials, etc. [11]. With the increase in the number of disturbances causing factors, the reflected waves become more and more complex due to the superimposition. The interpretation of these complex representations requires prior knowledge and experience, or if the tentative subsurface elements are known before the scan, they could be first scanned and analyzed in a control setup in a testing laboratory, and later the site data can be compared and controlled test data and interpreted. A processed data of a scan done on a pavement and the interpretation (which is not

drawn to the same scale as that of the scan) is shown in Fig. 7.

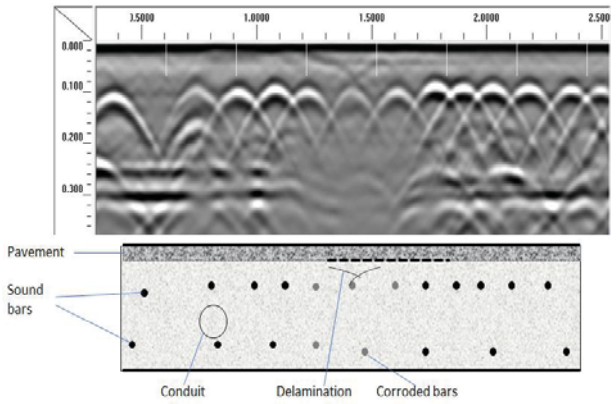

Fig. 7. Processed GPR data (top) and its interpretation (bottom). (The interpretation image is not drawn to scale)

C. *Void Detection*

GPR systems emit waves, and the antennas detect the reflected waves typically in homogenous media. Waves get reflected whenever there is a change in the medium occurs along the direction of propagation of waves. Any object with a dimension greater than the wavelength of the emitted Electromagnetic waves would reflect. So, not every crack or void would be identified in a single scan, instead, multiple scans of different wavelengths are required to detect all possible cracks. Every recorded data along each of the gridline are then merged to form a complete image, which is known as Radargram. The left of Fig. 8 shows the reflected wave obtained as a result of reflections on multiple layer interfaces and the right image shows the radargram obtained by merging several such series of recorded reflected wave data [13].

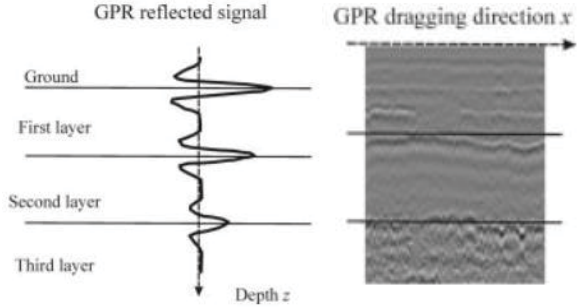

Fig. 8. The reflected wave pattern of a single wave (left) and radargram (right), image source [13]

Consider a concrete element with a void in it. Voids could be either filled with water or air, which is a different medium to that of concrete. So, in the similar fashion, waves would be reflected, and voids can be detected in a spatial coordinate system [13]. Fig. 9 illustrates two different reflected wave patterns that could be obtained from two different sizes of voids.

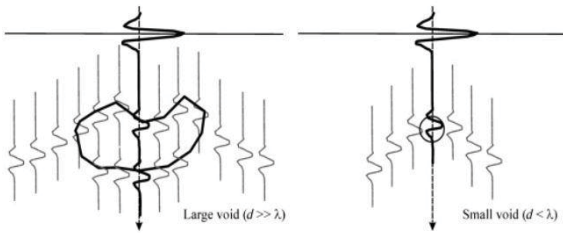

Fig. 9. Reflected wave patterns from voids of two different sizes, image source [13].

III. Proposed Methodology

A. *Reconstruction of representative Point cloud*

LiDAR produces point cloud data only as a surface representation, but GPR produces data to represent the subsurface characteristics. There are instances where other sensors and radars are used along with LiDAR to obtain different combinations of results along with the surface details [14,15].

Consider a homogenous concrete beam element of dimensions 0.3 m x 0.5 m x 2 m. Using Matlab as the tool of choice, synthetic point clouds were created as solid 3D Point Cloud data instead of conventional 2.5D. This representation is not valid if LiDAR alone is used in real life but when we combine the GPR data with LiDAR data, this is a realistic geometry representation. Fig. 10 shows the point cloud representation of the aforementioned beam.

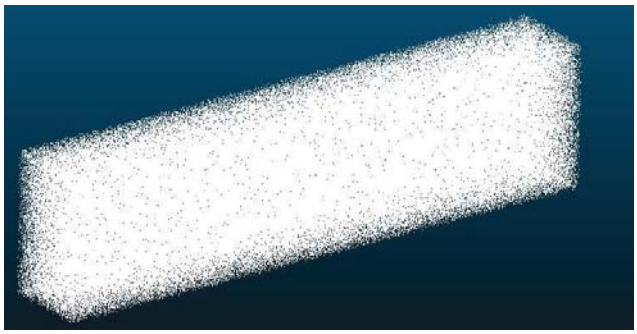

Fig. 10. Point cloud representation of the considered beam element. reproduced using CloudCompare software.

Point density is one of the important parameters in a point cloud. The higher the point density, the better the results are. But having high point cloud density would be computationally expensive and may contain unnecessary data, which needs to be eliminated before making it into a usable form [12,21]. Fig. 11 shows four Point Cloud representations of the same beam but with different Point densities.

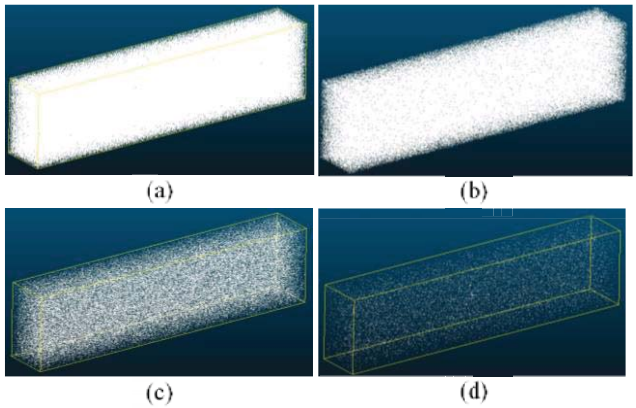

Fig. 11. Point Clouds with different Point densities, (a) 1000000 (b)500000 (c)100000 and (d)10000 points, recreated using CloudCompare.

B. *Introducing voids to the beam*

Honeycombs in a concrete structure are voids that are created due to improper casting of concrete [1]. The

honeycombs are idealised as voids and for the analysis purpose, hollow spheres are introduced to the beam to represent the honeycombs [2]. This was created by initially defining a random matrix with three columns (representing the spatial coordinates x, y and z of the points) and rows equal to the density of the point cloud (say n), such that the dimension of the random matrix becomes 3xn. Chosen point cloud densities for the analysis were 200,000, 500,000, 1,000,000 and 2,000,000. Later, six centres (x_i, y_i, z_i) were selected at two different levels of the beam (3 centres in each level) at sufficiently enough spacing, so that the created spheres will not overlap on each other. Spheres were later introduced while the centres of the spheres lie on the selected 6 centres and with defined radii. Selected radii for the analysis were 1cm, 2cm, 4cm, 6cm, 8cm and 10cm. This was done using an algorithm developed in MATLAB R2021a. Later the matrices were exported as ASCII files and fed as the input for the CloudCompare software for the cloud-to-cloud comparisons The positions of the spheres are depicted in Fig. 12 which is a sectional cut created using SOLIDWORKS software (only for demonstration purpose and drawn to the same scale as that of the created synthetic point cloud). All spheres are embedded within the beam, thus in real-life these voids cannot be seen.

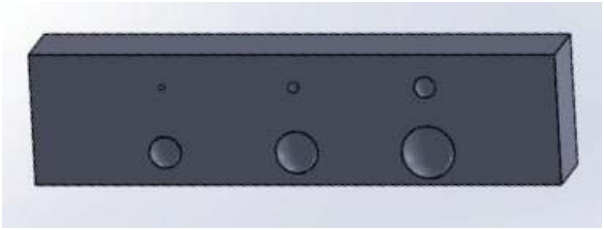

Fig. 12. The beam with voids of diameters 10 cm, 8 cm, 6 cm, 4 cm, 2 cm and 1 cm.

The synthetic point cloud representation of the beam that we created earlier is taken as the reference point cloud for the comparison and this can be created for any geometry comfortably using any 3D modelling software and later can be converted as a point cloud.

Meanwhile, another point cloud with voids embedded in the beam is also created. Fig. 13 shows the point cloud of the beam embedded with the voids. It is clearly understood that the voids that are embedded into the beam would not be visible for naked eyes, which is a similar case when there are honeycombs inside concrete structures.

C. Cloud-to-Cloud Comparision

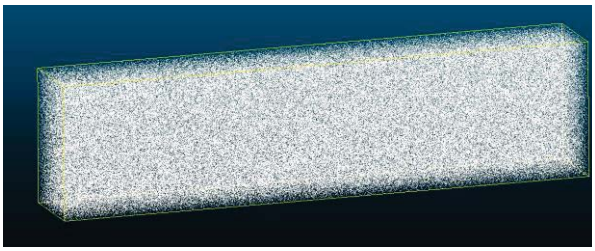

Fig. 13. Point Cloud of the beam with Voids embedded, created using Matlab and visualized in CloudCompare.

Cloud-to-Cloud comparison is a technique in which two selected point clouds can be compared to detect any changes. It works reliably only when the two point clouds can be aligned to each otherwise there could be a significant discrepancy in the results. One point cloud is considered as a *Reference* Point cloud, whereas the other is the *Compared* point cloud. The principle behind the comparison is, finding the nearest neighbour distance to compute the distance between two points, one from the reference point cloud and another from the compared point cloud [13]. The mathematical principle used to compute the Cloud-to-Cloud distance is a part of the Hausdorff Distance algorithm [20]. The x and y are elements of the subsets X and Y of a metric space. Distances between a point from subset X to all the points from subset Y is calculated and the highest lower bound, the infimum, is determined. Here sets X and Y are the two point clouds selected for the comparison. The generalized equation that is utilized in the CloudCompare software is given as in (1), here 'a' is an element of the set A (reference point cloud), 'b' are the elements of set B (compared point cloud), and A and B are subsets of metric space.

$$d(a,B) = \inf \{d(a,b) \mid b \in B \} \quad (1)$$

The distance calculated using Equation (1) can be interpreted as the distance from any points 'a' from the reference point cloud to another point from the compared point cloud. The point in the reference point cloud would be the nearest of all the points from the other point cloud. To make the calculation process quicker, the maximum distance can be set by the user [20], such that the distance calculation is restricted inside a sphere of radius equivalent to the maximum distance provided by the user and having the point 'a' as the centre of the sphere. A 2-dimensional visual representation of Equation (1) is given in Fig. 14 for better understanding.

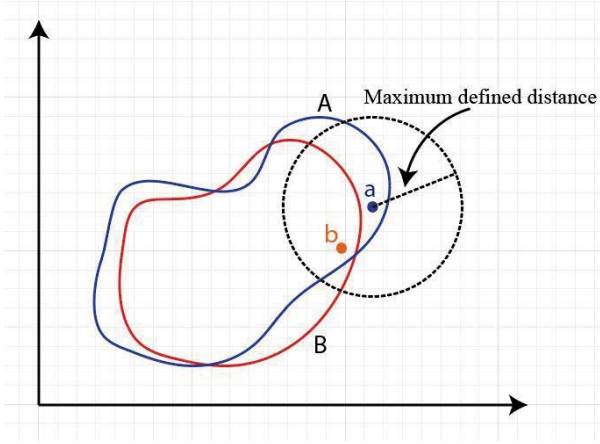

Fig. 14. 2D visual representation of the algorithm used in CloudCompare for Cloud-to-Cloud distance calculation.

All the results that are provided in this paper are the outputs of the Cloud-to-Cloud comparison done using CloudCompare software and a sample of the results along with the distance spectrum is provided in the latter part of the paper.

The results obtained after Cloud-to-Cloud comparison in the CloudCompare software is shown in Fig. 15. Fig. 15 (a) represents the voids introduced at the upper level of the beam section (smaller voids), while Fig. 15 (b), represents the voids introduced at the lower level of the beam section (larger voids) respectively. According to the comparison done using the CloudCompare software for the reference point cloud and point cloud with voids, at the point cloud density of 500,000 points, the voids of diameter less than 2cm are barely visible in Fig. 15 (a).

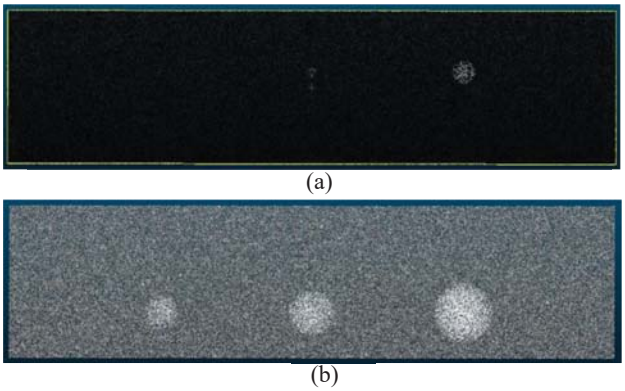

(a)

(b)

Fig. 15. Results of the Cloud Compare, obtained using

Since the voids of diameter less than 2 cm were undetected in the comparison done at a density of 500,000 points, those three voids were again compared using point cloud densities of 100,000, 1,000,000 and 2,000,000. According to the comparison results obtained using CloudCompare, by increasing or reducing the point cloud density from a density of 500,000 points, the void identification did not show any significant improvement. Also, with the increase and decrease in the point cloud density, the void corresponding to 4 cm diameter tends to diminish. Therefore, finding an optimum point cloud density for the purpose depends on the time and availability of resources to obtain dense point clouds, if required. The Cloud-to-Cloud comparison results obtained using CloudCompare software are shown in Fig. 16.

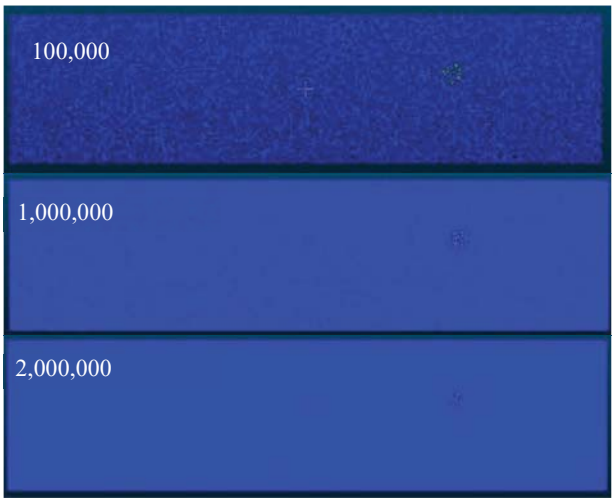

Fig. 16. Cloud-to-Cloud comparison results for different point cloud densities, obtained using CloudCompare.

The comparison was done repeatedly by changing the maximum distance to be detected during the Cloud-to-Cloud comparison at an expense of time taken for the completion of the analysis. The analysis was done using point clouds with 500,000 and 2,000,000 points with a maximum detection distance of 0.005 m and the results are shown in Fig. 17. When the maximum distance is reduced to 0.5 cm, the 2 cm diameter void became visible and it is noticeable in Fig. 17 irrespective of the point cloud density, though the 1 cm diameter void was barely visible.

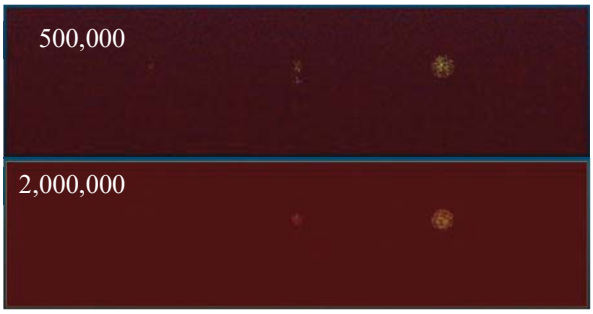

Fig. 17. Cloud-to-Cloud comparison for 500,000 and 2,000,000 point cloud densities at 0.005m maximum distance level, obtained using CloudCompare.

D. Extracting the Voids from the Reference Point Cloud

Even though the results obtained using CloudCompare software after Cloud-to-Cloud comparison are satisfactory to observe voids visually, it may not always be possible to identify voids that are embedded deeper in the concrete element with relatively larger section size, because the points that are at the surface often conceal the points below the dense point cloud.

To overcome this issue, a different approach was formulated. Using Matlab and CloudCompare together, we have developed a simple filtration to extract the voids from the reference point cloud. It is possible since the after-comparison results from CloudCompare software provides the data of the distance between each point in the reference point cloud to that of the nearest point in the compared point cloud, the distance is often represented as a spectrum as shown in Fig. 18.

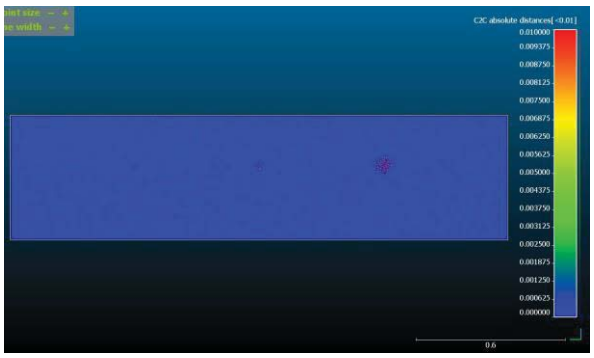

Fig. 18. Cloud-to-Cloud comparison results, obtained using CloudComapre.

First, the output of the Cloud-to-Cloud comparison from CloudCompare is obtained as an image format. An image file can also be represented in terms of pixel data, which contain spatial coordinates of each pixel (x,y,z) and the RGB values of each pixel, in other words, pixel data is a matrix representation of an RGB image, with 6 columns and rows equal to the number of pixels in the image. Then using the pixel data the points are filtered based on the colours using Matlab as a tool. Here the filtration should be done based on the dimension of the voids that the user is required to check. Then the filtered points are exported as a separate Point Cloud, which contains only the points from the reference point cloud, which have higher or equal Cloud-to-Cloud distance as mentioned by the user in the filtration, which interprets the voids in the concrete beam element that we considered in the study. Using this extracted point cloud, identification of voids at any depth is possible. The extracted point cloud is shown in Fig. 19.

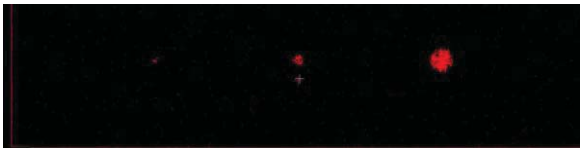

Fig. 19. Extracted points corresponding to the voids, obtained using Matlab software

The pixel filtration approach proposed in this paper is given in Fig. 20.

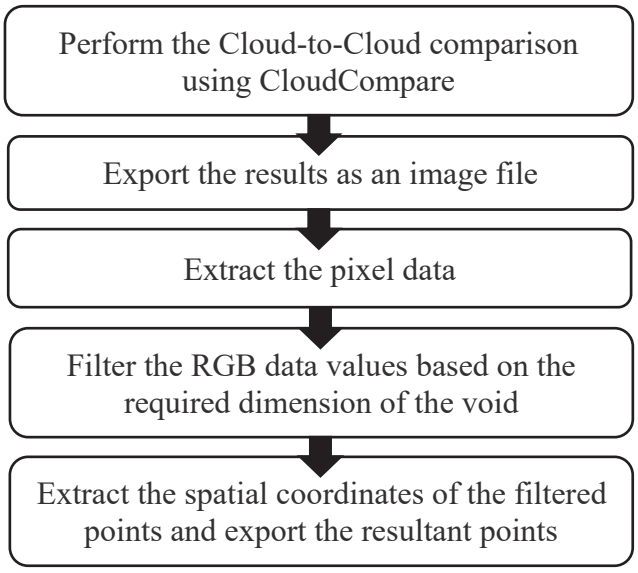

Fig. 20. Flow chart of the performed filtration algorithm

Extracting the points corresponding to the voids as a separate point cloud have tremendous advantages, the continuity of voids can be easily discovered, the severity of the honeycombs can be identified and further inspected. If these combined scans are performed in newly built structures, not only the results can be used to identify the defects, also can be used as a digital twin of the structure and the data can be submitted for the as-built drawing submissions which are often required at the end of the construction and handing over phase [21].

IV. Discussion

GPR and LiDAR are two different technologies/tools that are widely used in several instances and so far, they have been used independently. GPR is generally used to perceive the subsurface conditions, whereas LiDAR is used for the surface reconstruction of objects. GPR could not be used for surface reconstruction, while LiDAR could not be used for subsurface detail extraction are the drawbacks that could be eliminated when both are used in combination. Because LiDAR is a tool that can be utilized to compare the as-built and as-planned structures in the Civil Engineering industry [21], but it only compares the surface alignments. But when paired with GPR and the output of the GPR data is converted to point cloud format and merged with the LiDAR point cloud output, a full 3-dimensional reconstruction of the whole structure is possible, and this would lead to easy identification of subsurface and surface defects in the elements of the structure in terms of quality control. The scope of this research paper was narrowed down to verify the usability of Point cloud in only honeycomb detection and illustrated using synthetic point cloud of a beam element with and without artificially introduced voids embedded into the beam, which corresponds to the honeycombs in real life [2]. Since the actual geometry of the elements would be known in a real-life scenario, it is possible to create synthetic point clouds using the method proposed in this paper as a reference point cloud and the data for the real elements can be obtained by both LiDAR and GPR scans, which will represent the compared point cloud.

The analysis conducted is made as realistic as possible and since the target criteria are well constrained, the idealization is valid for the selected case. Using CloudCompare as a tool, both the synthetic point clouds (reference and compared point cloud) were visualized and compared. The comparison made it possible to identify voids of diameter 2 cm and greater, and void of diameter 1cm was barely visible in the compared point cloud, but in a real test case, when the locations of the voids are unknown and other disturbances are present, it may be difficult to interpret the 1cm range voids as voids. Using CloudCompare, section slices can be obtained in places where required and a sample of a section slice is shown in Fig. 21.

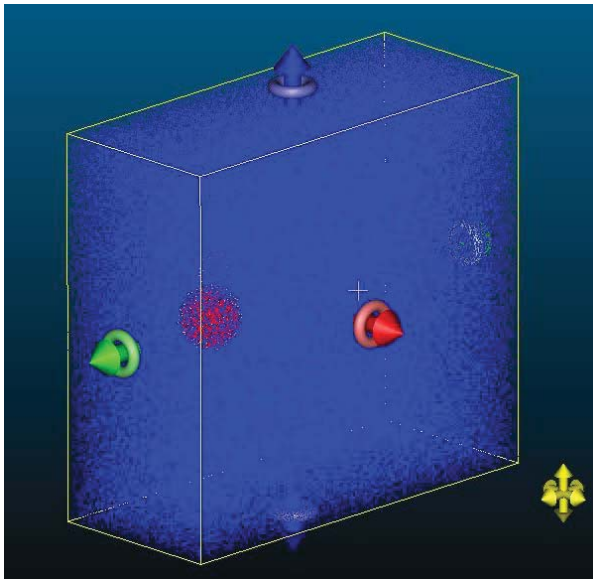

Fig. 21. Section slice of the beam section and the 0.04m void, obtained using CloudCompare.

Even though point cloud can be used to detect honeycombs in concrete while used together with GPR as explained in this paper, the output of the GPR plays a major role. Detection of voids depends on the wavelength of the GPR signal [13] and other abnormalities. With the increase of abnormalities, the reflected wave becomes more complex. When the abnormalities are known to a certain extent, in the case of concrete elements, we can remove unwanted abnormalities in the Point cloud and use the rest for further analysis. In a field and lab test conducted using only GPR, GPR showed promising results in finding voids as small as 3.2 cm in dimension during the early stage of the concrete (before the setting of concrete) [18]. According to a field test experiment conducted as in [19], only the GPR survey was done using two different frequencies, 450 MHz and 900 MHz and the results were compared. The results of 450 MHz showed stronger reflections from the rebars, less or no reflections from the top of the voids and no reflection from the bottom of the concrete slab but 900 MHz results

defined the top of the voids clearly and the bottom of the concrete slab. Therefore, conducting scans at two different frequencies would help identify the location and arrangements of the rebars and the voids underneath the rebars, and most importantly selection of the frequency play a major role in the output of the GPR. By increasing the frequency of the GPR system, even fine cracks can be detected but it requires a detector at the opposite side of the scanner, which is not considered in the scope of this research paper.

To implement this in real-world scenarios, the LiDAR point cloud data and the GPR output data are required in addition to the dimension details of the elements under consideration. With the dimensions and the shape of the elements are known, a synthetic point cloud can be created as the reference point cloud. This will well suit linear elements such as beams, slabs, walls and columns. Meanwhile, the GPR output can also be converted as a point cloud output. By using CloudCompare as a tool, the point cloud of the GPR output and the reference synthetic point cloud can be compared and visualized. Then the output of the CloudCompare could be obtained in image formats and the points corresponding to the honeycombs can be separated using the pixel data filtration approach as mentioned in this paper. To reconstruct a complete 3D representation of the structure or the elements, the extracted point cloud from the filtration process can be aligned with the LiDAR point cloud output, so that now the aligned point cloud consists of both surface details and the subsurface details (honeycombs, rebars, cracks, foreign particles, etc) simultaneously. This would aid during the quality control procedures (easy detection of the location and size of the honeycombs) and the as-built vs as-planned model or drawing preparations.

V. Conclusion

This paper clearly shows the possibility for the use of GPR and LiDAR together for better honeycomb detection and produce a full 3-dimensional representation of the whole structure or individual elements using synthetic point clouds and the advantages of using point cloud in honeycomb detection. From the comparison results obtained from CloudCompare, the following conclusions are made.

1. The synergy of GPR and LiDAR allows the digital recognition of voids in concrete and 3D reconstruction of concrete structures or elements rather than 2.5D representations.
2. The density of the point clouds influences the easy detection of the voids; higher point cloud density could conceal the voids underneath, whereas point cloud with lower density could produce inaccurate or unreliable outputs.
3. By adjusting the maximum distance during the cloud-to-cloud comparison in CloudCompare, void detection can be improved, and the computation time can be reduced.

For the considered beam, void of diameter 2 cm is visible for point cloud of the density of 2,000,000 points than point cloud of density 500,000 and the void corresponding to 0.01 m is barely visible for point cloud of density 2,000,000, at a maximum distance of 0.5 cm. Even though there are restrictions for the GPR signal travel depth in objects, since the study is mainly focused on concrete structures, there are possibilities to access the elements from several directions. Meanwhile, when the GPR output is combined with LiDAR data, a complete Point Cloud representation of concrete elements or a complete structure can be obtained. Using this combined result, the honeycombs, both internal and surface honeycombs, can be easily figured out in terms of their locations and their dimensions. From this, an analyst would be able to determine which voids are at critical locations, which reduces the time of going through every scanned output and locating their relative locations in the structure.

Acknowledgement

The authors of the paper gratefully acknowledge the support and guidance given by the staff member of Murphy Geospatial and Dr Wayne B Muller.

References

[1] Völker, C., & Shokouhi, P. (2015). Multi sensor data fusion approach for automatic honeycomb detection in concrete. NDT & E International, 71, 54-60.

[2] Trela, C., Kind, T., & Schubert, M. (2015, July). Detection of air voids in concrete by radar in transmission mode. In 2015 8th International Workshop on Advanced Ground Penetrating Radar (IWAGPR) (pp. 1-4). IEEE.

[3] Mishra, G. (2019, April). Honeycombs in Concrete – Their Causes and Remedies. The Constructor. https://theconstructor.org/practical-guide/honeycombs-in-concrete-and-remedies/6889/

[4] Cafiso, S., Di Graziano, A., Goulias, D., Mangiameli, M., & Mussumeci, G. (2020). Implementation of GPR and TLS data for the assessment of the bridge slab geometry and reinforcement. Archives of Civil Engineering, 66(1).

[5] Giannopoulos, A. (2005). Modelling ground penetrating radar by GprMax. Construction and building materials, 19(10), 755-762.

[6] Greif, T., Stein, N., & Flath, C. M. (2020). Peeking into the void: Digital twins for construction site logistics. Computers in Industry, 121, 103264

[7] El-Omari, S., & Moselhi, O. (2008). Integrating 3D laser scanning and photogrammetry for progress measurement of construction work. Automation in construction, 18(1), 1-9.

[8] Walsh, S. B., Borello, D. J., Guldur, B., & Hajjar, J. F. (2013). Data processing of point clouds for object detection for structural engineering applications. Computer‐Aided Civil and Infrastructure Engineering, 28(7), 495-508.

[9] Brenner, C. (2005). Building reconstruction from images and laser scanning. International Journal of Applied

[10] Halabe, U. B. (2013). Non-destructive evaluation (NDE) of composites: techniques for civil structures. In Non-Destructive Evaluation (NDE) of Polymer Matrix Composites (pp. 483-517e). Woodhead Publishing.

[11] Penetradar.com. 2021. GPR Inspection Vehicles – Penetradar. [online] Available at: <http://penetradar.com/new/?page_id=525> [Accessed 5 July 2021].

[12] Rasol, M. A., Pérez-Gracia, V., Fernandes, F. M., Pais, J. C., Santos-Assunçao, S., Santos, C., & Sossa, V. (2020). GPR laboratory tests and numerical models to characterize cracks in cement concrete specimens, exemplifying damage in rigid pavement. Measurement, 158, 107662.

[13] Hashmi, S. (2014). Comprehensive materials processing. Newnes.

[14] Narváez, F. J. Y., del Pedregal, J. S., Prieto, P. A., Torres-Torriti, M., & Cheein, F. A. A. (2016). LiDAR and thermal images fusion for ground-based 3D characterisation of fruit trees. Biosystems Engineering, 151, 479-494.

[15] Comstock, J. M., Ackerman, T. P., & Mace, G. G. (2002). Ground‐based lidar and radar remote sensing of tropical cirrus clouds at Nauru Island: Cloud statistics and radiative impacts. Journal of Geophysical Research: Atmospheres, 107(D23), AAC-16.

[16] Kim, M. K., Cheng, J. C., Sohn, H., & Chang, C. C. (2015). A framework for dimensional and surface quality assessment of precast concrete elements using BIM and 3D laser scanning. Automation in Construction, 49, 225-238.

[17] Antova, G. (2019). Application of areal change detection methods using point clouds data. In IOP Conference Series: Earth and Environmental Science (Vol. 221, No. 1, p. 012082). IOP Publishing

[18] McCabe, T., Erdogmus, E., Kodsy, A., & Morcous, G. (2021). Early Detection of Honeycombs in Concrete Pavement Using GPR. Journal of Performance of Constructed Facilities, 35(1), 04020138.

[19] Cassidy, N. J., Eddies, R., & Dods, S. (2011). Void detection beneath reinforced concrete sections: The practical application of ground-penetrating radar and ultrasonic techniques. Journal of Applied Geophysics, 74(4), 263-276.

[20] *Cloud-to-Cloud Distance - CloudCompareWiki*. (n.d.). CloudCompare. Retrieved July 28, 2021, from https://www.cloudcompare.org/doc/wiki/index.php?title=Cloud-to-Cloud_Distance

[21] Subakaran, R., & Herath, H. M. S. T. (2021). Feasibility of using 3D point cloud technologies in Sri Lankan Civil Engineering Industry. *Modulus*, *31*(01), 19–25. http://dl.lib.uom.lk/handle/123/16510

[22] *MATLAB Documentation - MathWorks India*. (n.d.). MathWORK. Retrieved May 10, 2021, from https://in.mathworks.com/help/matlab/

[23] *Cloud Compare V2.6.1-User Manual(huhongjun)*. (n.d.). UserManual.Wiki. Retrieved May 10, 2021, from https://usermanual.wiki/Document/CloudCompareV261User20manualhuhongjun.1487341153/html

[24] *Manual Download - 2019 - SOLIDWORKS Help*. (n.d.). DASSAULT SYSTEMS. Retrieved May 10, 2021, from https://help.solidworks.com/2019/english/SolidWorks/install_guide/HID_STATE_MANUAL_DOWNLOAD.htm

[25] *User Manuals*. (n.d.). Agisoft. Retrieved May 10, 2021, from https://www.agisoft.com/downloads/user-manuals/